Available online at www.sciencedirect.com

ScienceDirect

www.elsevier.com/locate/jes

JES JOURNAL OF ENVIRONMENTAL SCIENCES

www.jesc.ac.cn

Synthesis of highly effective absorbents with waste quenching blast furnace slag to remove Methyl Orange from aqueous solution

Hongyu Gao[1,2], *Zhenzhen Song*[3], *Weijun Zhang*[4,*], *Xiaofang Yang*[2], *Xuan Wang*[1], *Dongsheng Wang*[1,2,*]

1. *Faculty of Materials Science and Chemistry, China University of Geosciences, Wuhan 430074, China*
2. *State Key Laboratory of Environmental Aquatic Chemistry, Research Center for co-Environmental Sciences, Chinese Academy of Sciences, Beijing 100085, China*
3. *Technology Center, ZhongYang Steel Co., Ltd., Zhongyang 033400, China*
4. *School of Environmental Studies, China University of Geosciences, Wuhan 430074, China*

ARTICLE INFO

Article history:
Received 3 March 2016
Revised 23 May 2016
Accepted 24 May 2016
Available online 14 June 2016

Keywords:
Water-quench blast furnace slag
BFS micro powder
Modified BFS
Methyl orange decolorant
Adsorbability

ABSTRACT

Water quenching blast furnace slag (WQBFS) is widely produced in the blast furnace iron making process. It is mainly composed of CaO, MgO, Al_2O_3, and SiO_2 with low contents of other metal elements such as Fe, Mn, Ti, K and Na. In this study, WQBFS was treated with grinding, hydrochloric acid acidification, filtration, filtrate extraction by alkali liquor and a hydration reaction. Then BFS micropowder (BFSMP), BFS acidified solid (BFSAS) and BFS acid-alkali precipitate (BFSAP) were obtained, which were characterized by X-ray diffraction, scanning electron microscopy, X-ray fluorescence and Brunauer-Emmet-Teller (BET) specific surface area. The decoloration efficiency for Methyl Orange (MO) was used to evaluate the adsorptive ability of the three absorbents. The effects of adsorptive reaction conditions (pH and temperature of solution, reaction time, sorbent dosage and initial concentration) on MO removal were also investigated in detail. The results indicated that BFSAP performed better in MO removal than the other two absorbents. When the pH value of MO solutions was in the range 3.0–13.0, the degradation efficiency of a solution with initial MO concentration of 25 mg/L reached 99.97% for a reaction time of 25 min at 25°C. The maximum adsorption capacity of BFSAP for MO was 167 mg/g. Based on optimized experiments, the results conformed with the Langmuir adsorption isotherm and pseudo-second-order kinetics. Among inorganic anions, SO_4^{2-} and PO_4^{3-} had significant inhibitory effects on MO removal in BFSAP treatment due to ion-exchange adsorption.

© 2016 The Research Center for Eco-Environmental Sciences, Chinese Academy of Sciences. Published by Elsevier B.V.

Introduction

Blast furnace slag (BFS) is a co-product of the iron manufacturing process. According to the control mode used for cooling rate and time, it can be divided into water quenching blast furnace slag (amorphous state) and air cooling blast furnace slag (crystalline state). Whether in the amorphous or crystalline state, the slags have similar chemical components and mainly contain CaO, MgO, Al_2O_3, SiO_2, and other minor components such as Fe_2O_3, MnO_2, K_2O, Na_2O and TiO_2. Since the water

* *Corresponding authors.* E-mails: zhwj_1986@126.com (Weijun Zhang), wgds@rcees.ac.cn (Dongsheng Wang).

http://dx.doi.org/10.1016/j.jes.2016.05.014
1001-0742/© 2016 The Research Center for Eco-Environmental Sciences, Chinese Academy of Sciences. Published by Elsevier B.V.

quenching technology has the advantages of simple operation, lower space requirements, low cost and fast processing time, more than 75% of iron and steel enterprises adopt this technique to treat blast furnace slag in China. In 2014, the global output of pig iron output was 1.179 Gt, with China accounting for more than 60%. According to empirical calculations, the BFS production is approximately 400 kg/ton pig iron. A large amount of BFS not only requires space to store and manage, but also causes serious environmental pollution (water, air and soil). Therefore, comprehensive utilization and recycling of BFS is very crucial for sustainable development of steel enterprises (Yang et al., 2013; Ren et al., 2014; Yan, 2012; Chen and Liu, 2007).

Methyl Orange (MO) is a typical dye and has been widely used in many industrial processes. MO-containing wastewater is toxic and resistant to biodegradation. Thus, many physicochemical methods have been developed to remove MO from aqueous solution. Adsorption processes have many advantages including simple operation, high efficiency, fast reaction and so on. The developed adsorbents for MO removal include synthesized metals/semiconductors, oxide/graphene nanocomposites, metal oxide/nano-size materials, metal oxide/porous materials and porous materials. In photo-catalytic processes, metal oxides have been loaded on the surface of natural or synthetic ores to decompose H_2O_2 to form hydroxyl radicals (Wang et al., 2015; Zheng et al., 2015; Dou et al., 2015; Barbosa et al., 2015). In general, these materials, such as activated carbon, zeolite, rare earth, kaolin, diatomite, et al., exhibit a porous structure and large specific surface area. Adsorption of MO has been studied using layered double hydroxides (LDH), layered double oxides (LDO) and hydrotalcite-like materials in acidic conditions, under certain conditions of reaction time and temperature (Zhang et al., 2014a; Kuwahara et al., 2013; Wang et al., 2015). As-prepared ZnAl-LDHs and LDOs showed excellent adsorption capacity toward MO in aqueous solution (Li et al., 2014). The adsorption behavior and mechanism of reactive brilliant red X-3B in aqueous solution over three kinds of hydrotalcite-like LDHs and found that these hydrotalcite-like LDHs have a relatively high adsorption rate in the pH range of 3–9 (Zhang et al., 2014b). The red dyes (Reactive Red, Congo Red and Acid Red 1) were removed efficiently by Mg–Al-LDH, and showed clearly that the optimal dosage and contact time for Mg–Al-LDH were 0.10 g and 60 min, and that pH had little effect at pH < 10 (Shan et al., 2015).

In this study, our aim was to use waste blast furnace slag to synthesize absorbents to remove MO from aqueous solution. In detail, the waste blast furnace slag was treated and synthesized into three materials (BFS micropowder (BFSMP), BFS acidified solid (BFSAS) and BFS acid-alkali precipitate (BFSAP)). These materials were characterized by X-ray diffraction, BET surface area and scanning electron micrograph. Their adsorptive ability for MO removal was compared according to decoloration effectiveness. In addition, the effect of reaction conditions (pH, temperature, initial MO concentration, inorganic anions) on MO removal was also investigated. This study aimed to provide a feasible solution for synthesizing adsorbents from waste BFS for MO-containing wastewater treatment.

1. Materials and methods

1.1. Sample description

All chemicals used were of analytical grade and supplied by Sinopharm Chemical Reagent Co., Ltd. WQBFS was supplied by the ZhongYang Steel Co., Ltd., China and its chemical composition is given in Table 1. Ultra-pure (UP) water was used throughout the experiments.

1.2. BFS pretreatment

WQBFS was ground by a ball mill to a particle size less than 38 μm to give BFSMP. BFSMP (10.0 g) and hydrochloric acid (200 mL, 3 mol/L) were mixed in a conical flask and covered with sealing film, and kept for 2 hr in a 95°C water bath. The insoluble solid was separated with a filtration membrane and then washed with ultra-pure water, then the solid residuals were dried and collected as BFSAS. Then, the pH of the supernatant was adjusted to 11.0 ± 0.1 using 0.8% sodium hydroxide solution and covered with sealing film, and kept for 18–20 hr in a 60°C water bath. The suspension was centrifuged to separate the sediments, which were dried at −55°C with a freeze–drier and then collected as BFSAP for use (Fig. 1).

1.3. Adsorption experiment with Methyl Orange solution

MO solutions were prepared at concentrations of 0.0 mg/L, 0.5 mg/L, 1.0 mg/L, 1.5 mg/L, 2.0 mg/L, 2.5 mg/L, 4 mg/L and 8 mg/L, respectively. The absorbance of the solutions was determined using a double-beam UV–Vis spectrophotometer to construct a standard curve for MO quantification in the following work.

BFSMP, BFSAS and BFSAP of different doses were placed into the prepared series of MO solutions in 50 mL colorimetric tubes respectively. The tubes were then stirred for 30 min at 25°C in a gas bath thermostatic oscillator at a constant shaking rate. The absorbents were removed with a syringe with filter and the absorbance was measured using a double-beam UV–Vis Spectrophotometer.

Table 1 – Chemical composition of blast furnace slag (BFS) micropowder (BFSMP), BFS acidified solid (BFSAS) and BFS acid-alkali precipitation (BFSAP).

Compound	BFS (Unit status, %)	BFSAS (Unit status, %)	BFSAP (Unit status, %)
SiO_2	32.01	86.79	0.00
Al_2O_3	14.94	0.49	18.30
Fe_2O_3	0.31	0.02	0.34
MgO	9.55	0.33	24.93
CaO	36.11	1.32	11.92
Na_2O	0.23	0.02	14.19
K_2O	0.22	0.02	0.37
MnO	0.46	0.03	0.51
TiO_2	1.15	0.16	1.10
P_2O_5	0.01	0.01	0.01
CO_2	0.00	0.00	15.42
H_2O	5.01	10.81	12.91

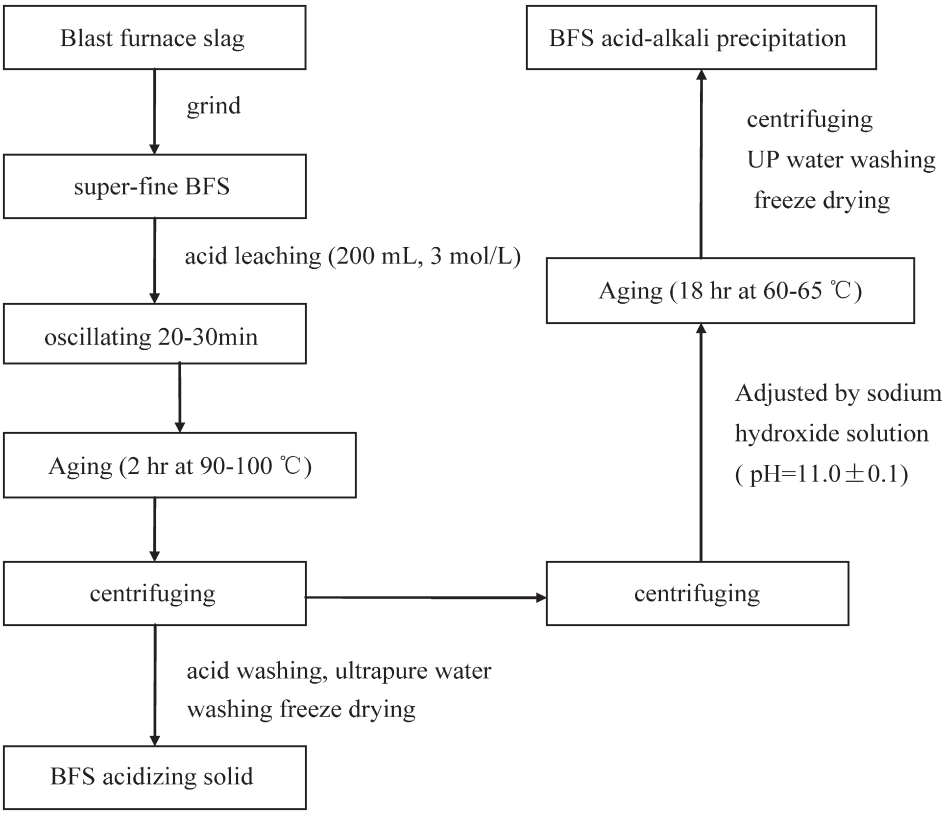

Fig. 1 – Treatment procedure of water quenching blast furnace slag.

In each of the batch adsorption experiments, 40 mL of MO solution of known initial concentration (20–150 mg/L) was treated by a specified known dosage of BFSMP, BFSAS or BFSAP (0.05–0.4 g). In addition, optimization experiments were performed by changing the process parameters such as pH (1–13), BFSMP, BFSAS and BFSAP dosages, initial MO concentration (25–150 mg/L), and reaction time (1–30 min). After adsorption equilibrium was reached, the supernatant was separated from the reaction system using a syringe with filter (average pore diameter 0.22 μm). The MO content in the filtrate was analyzed by a double-beam UV–Vis spectrophotometer at 474 nm (U-2910, Hitachi, Japan). The MO adsorption rate (η, %) was calculated using the equation:

$$\eta = \frac{c_0 - c_e}{c_0} \times 100\% \quad (1)$$

where c_0 (mg/L) and c_e (mg/L) respectively are the initial and final concentrations of MO in solution.

At equilibrium reaction time (t_e), the amount of MO at adsorption equilibrium (q_e) was calculated using the equation:

$$q_e = \frac{c_0 - c_e}{m} \times V_0 \quad (2)$$

where, V_0 (L) is volume of MO solution and m (g) denotes adsorbent dosage.

1.4. Analytical methods

The morphologies of super-fine BFS, BFSAS and BFSAP were observed with a scanning electron microscope (S-3000N, Hitachi, Japan). The resolution was 3.0 nm and the amplification factor was less than 300,000. The accelerating voltage was 3.0 kV.

X-ray diffraction (PANalytical, Netherlands) measurements were carried out with copper Ka radiation, utilizing a generator voltage of 40 kV and tube current of 40 mA. The divergence slit was fixed at 0.38 mm and data was collected for 2θ of 5–90° scanned at a rate of 5.48 deg/min.

The chemical compositions of the BFS, BFSAS and BFSAP samples were analyzed using X-ray fluorescence (XRF, SHIMADZU-EDX800, Japan), utilizing a generator voltage of 50 kV and tube current of 40 mA. The collimator diameter was 20 mm. Each sample was well mixed and analyzed three times.

Mid-infrared spectra were recorded using a Fourier transform infrared (FT-IR) spectrometer (Nicolet Nexus 370, Thermo, USA) with a Smart Endurance™ single bounce diamond ATR cell. Spectra were obtained from 4000 to 400 cm^{-1} by averaging of 64 scans with a resolution of 4 cm^{-1}. A mirror velocity of 0.6 cm/sec was used.

The BET surface area was determined as 57.84 ± 0.20 m^2/g with an ASAP 2000 instrument (Micromeritics, USA).

2. Result and discussion

2.1. Characterization of different BFSs

The N_2 adsorption–desorption isotherms of BFS, BFSAS and BFSAP showed type-IV isotherms with an H_2 hysteresis loop

as judged from Fig. 2. It is also noted that the width of the hysteresis loop increased with increasing pore volume. The mesopores had a regular framework with interparticle voids. In addition, the mesoporous material was prepared at acidic pH and a well-organized mesostructure even in the bulk state. The N_2 isotherm also showed that the porosity comprised uniform channels like the templated framework in silica monoliths (Awual and Hasan, 2014a, 2014b; Awual, 2014; E1-Safty et al., 2011). The BFSAS structure was successfully fabricated by using an acidizing method and exhibited favorable textural parameters for adsorption in terms of specific surface area (245 m^2/g), pore size (3.5 nm) and pore volume (0.18 cm^3/g), and BFSAP similarly exhibited appreciable textural parameters, with specific surface area 3.46 m^2/g, pore size 15.4 nm and pore volume 0.013 cm^3/g. The BFSMP sample exhibited less favorable textural parameters in terms of specific surface area (0.4 m^2/g), pore size (4.7 nm) and pore volume (0.005 cm^3/g) (Table 2).

Fig. 3a shows the SEM image of BFSMP, with various irregular amorphous particles having no pores and varied particle size. BFSMP was derived from broken WQBFS using a grinding miller. This means that the machine crushing process only changed the particle size, and the BET specific surface area was 1.28 m^2/g. The particle size varied and was less than or equal to 40 μm. It can also be observed that the surface of BFSMP was not smooth and the cross-section presented a flake structure. From Fig. 4, the X-ray diffraction (XRD) pattern of BFSAP shows the characteristic (003), (006) and (012) peaks of layered double hydroxides. On the basis of the data, we calculate and conjecture that BFSAP is a complex layered double hydroxide mixture.

As shown in Fig. 3b, BFSAS is porous and mainly composed of calcium silicate. It can be seen from Fig. 3c that BFSAP is porous and that the pore size varies greatly, and shows a layered structure.

In general, LDHs consist of positively charged metal hydroxide sheets with anions located within layers to compensate the positive layer charges. The composition of an LDH can be generally described by the formula as $[M^{2+}_{1-x}M^{3+}_x(OH)_2]^{x+}A^{n-}_{x/n}\cdot mH_2O$,

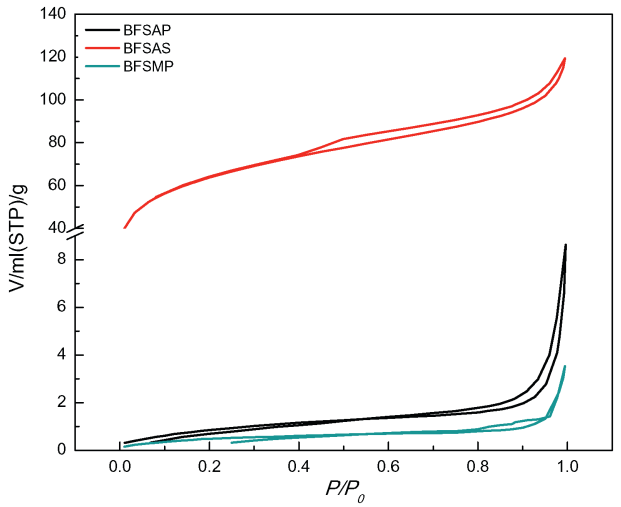

Fig. 2 – The curve graph of BET of three adsorbents (BFSMP, BFSAS and BFSAP).

Table 2 – The BET of BFSMP, BFSAS and BFSAP.

	BET (m^2/g)	V_P (cm^3/g) [a]	D (nm) [b]
BFSMP	0.40	0.005	4.7
BFSAS	245	0.180	3.5
BFSAP	3.46	0.013	15.4

[a] *Vp* is pore volume of BFSs.
[b] *D* is pore diameter of BFSs.

where M^{2+} represents divalent cations (Ca^{2+}, Mg^{2+}, Zn^{2+}, Fe^{2+}, Co^{2+}, Ni^{2+}, Cu^{2+}, Mn^{2+}), M^{3+} represents trivalent cations (Al^{3+}, Cr^{3+}, Fe^{3+}, Co^{3+}, Mn^{3+}), A^{n-} represents inorganic or organic anions (Cl^-, NO_3^-, ClO_4^-, CO_3^{2-}, SO_4^{2-}, $Zn(BPS)_3^{4-}$), *m* is the number of interlayer water molecules and *X* (=M^{2-} / (M^{2+} + M^{3+})) is the layer charge density of the LDH.

As depicted in Fig. 4, the basal spacing was calculated according to the position of the basal planes with the strongest XRD intensity, and the basal spacing of the synthesized LDHs was determined to be 7.80–7.91 Å (Kuwahara and Yamashita, 2015). XRD analysis revealed that the structure of BFSAP is similar to that of an LDH mixture but that it also contains K, Na, Fe, Ca, *etc.* According to chemical component analysis, BFSAP was mainly composed of $Mg_6Al_2(OH)_{16}Cl\cdot 4H_2O$ (7.84 Å) with a low content of $Mg_2Al_2(OH)_2Cl_4\cdot 15H_2O$ (7.62 Å) and $Ca_2Al(OH)_2Cl_5\cdot 4H_2O$ (7.86 Å). Again, a small amount of material containing CO_3^{2-} layers was detected because of absorption of CO_2 from the air in the process of preparation.

2.2. Effects of reaction conditions on removal efficiency of MO

2.2.1. Effect of adsorbent dosage on MO removal

The effects of absorbent dose on removal efficiency of MO can be found in Fig. 5. BFSAS and BFSAP performed much better in MO removal than BFSMP. For the BFSAS and BFSAP dosages of 0.1 g, the MO removal efficiency reached a maximum of 94% and 99% respectively. Adsorption efficiency remained unchanged with further increases of BFSAS and BFSAP dosages. BFSMP exhibited a very limited effect on MO adsorption regardless of its dose. Consequently, since BFSAP showed the most powerful absorptive ability for MO, it was used in the following experiments.

2.2.2. Effect of reaction temperature

The effects of temperature on MO removal are given in Fig. 6. It can be seen that the MO removal efficiency of BFSAS was reduced significantly from 96.1% to 49.4% with increasing temperature from 15 to 65°C, while the adsorption capacity of BFSAP for MO was very stable and more than 95% of MO was removed regardless of temperature. This result revealed that temperature has very limited effect on the adsorption of MO in BFSAP treatment.

2.2.3. Effect of pH on adsorption

In reports on treatment of simulated MO wastewater, the optimal pH has been in the acidic range (2–5). As shown in Fig. 7, the adsorption capacity of BFSMP for MO was very limited at various pH levels, and the maximum MO removal of 24% was reached at pH 3. The adsorption capacity of BFSAP toward MO increased with increasing pH. The MO removal

Table 3 – Adsorption capacity of various adsorbents for Methyl Orange (MO) removal.

Material	pH	Time (min)	Temperature (°C)	q_m (mg/g)	Reference
BFSAP	11.0–13.0	25	25	167	This study
FeOOH/CBC nanocomposite	4.0–6.0	60	30	107.68	Wang et al., 2015
Ni-Al LDH	5.0	–	50	186.4	Monash and Pugazhenthi, 2014
Zn-Al LDO	6.0	120	25	181.9	Ni et al., 2007
Polyacrylonitrile fiber	5.0	–	–	194	Fan et al., 2015

efficiency was 53% at pH of 1 and increased to 91%–92% in the pH range from 5 to 9. BFSAP was still very effective in MO removal and more than 98% of MO was removed at pH above 11.

However, the adsorption capacity of BFSAS for MO increased on raising pH from 1 to 5, and then decreased with further increase in pH from 5 to 13. A large amount of floccules was observed after addition of BFSAS. These results indicated that BFSAP was very effective in MO removal under strongly alkaline conditions. In most cases, dyeing wastewaters are alkaline, especially those of the sulfur dyes, and the pH of vat-dyeing wastewater is above 10. Hence, BFSAP is more favorable in dealing with alkaline dyeing wastewater and does not need a neutralization step prior to adsorption treatment.

From Fig. 8, it can be seen that the surface of BFSMP carried a negative charge, and BFSMP attracted positive charge. Moreover, BFSMP particles were essentially in a condensed state. BFSAS and BFSAP attracted anions because of the numerous positive charges on their surfaces. So these positively charged surfaces played a major role in the absorption of MO^-, and the positive charge of BFSAP was greater than BFSAS. However, with increasing pH, the dispersion of BFSAP and BFAS increased and BFSAS particles were essentially in a condensed state in alkaline conditions. Thus, MO^- was easily adsorbed by BFSAP and BFSAS. Because of the greater BET surface area of BFSAS, the MO adsorption of BFSAS was better than BFSAP in acidic conditions. When the pH value exceeded 7, the condensation of BFSAS particles and their lower positive charge led to worse MO adsorption than BFSAP.

2.2.4. Adsorption kinetics

The changes in MO removal efficiency and spectral absorption characteristics of MO solution are presented in Fig. 9a and b respectively. The MO removal of BFSAS and BFSAP increased with time and the adsorption process nearly reached equilibrium after 25 min, and BFSAS performed better than BFSAP in adsorptive treatment. In addition, BFSMP still showed little effect with increasing time. The adsorption processes of both BFSAP and BFSMP toward MO took place immediately, and 73.1% and 83.7% of MO was removed within 1 min respectively. In addition, the spectral absorption characteristics of the MO solution clearly revealed that BFSAP reached the maximum adsorption efficiency of 99.8% after 25 min. Kuwahara et al. (2010, 2013) also suggested that raw BFS showed a very limited effect on phosphate and organic removal. Adsorption of MO on pure FeOOH/CBC nanocomposite reached equilibrium after 60 min (Wang et al., 2015a, 2015b), which was much longer than that for BFSAP and BFSMP treatments in the present study.

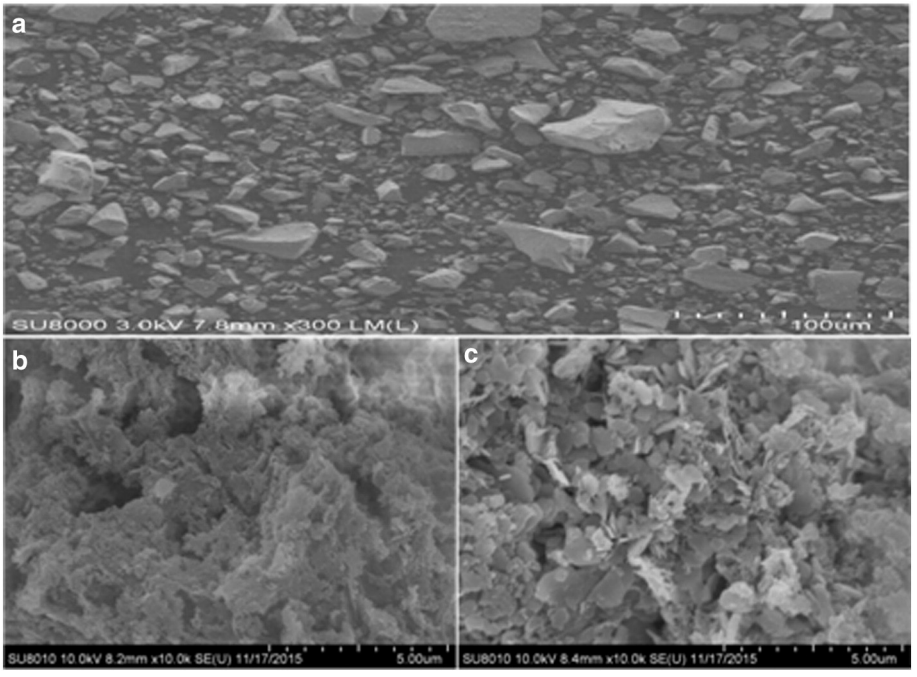

Fig. 3 – SEM imagines of BFSMP (a), BFSAS (b), and BFSAP (c).

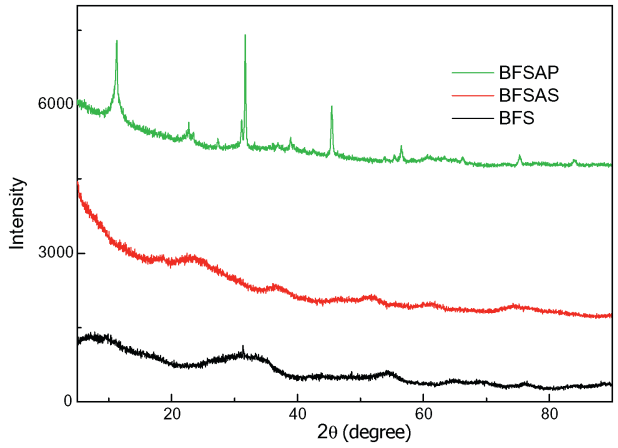

Fig. 4 – XRD spectra of BFSMP, BFSAS and BFSAP.

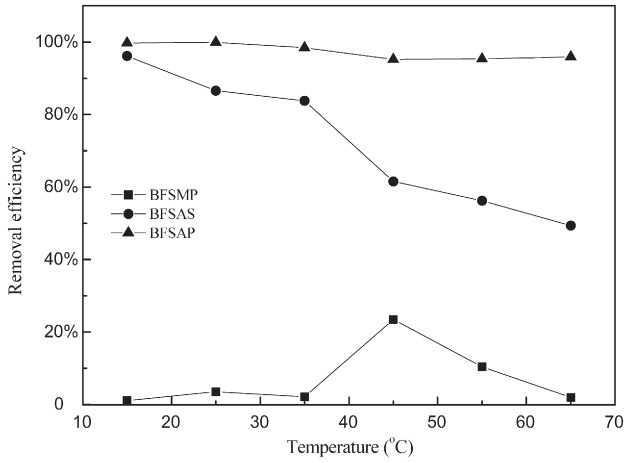

Fig. 6 – Influence of temperature on removal efficiency of MO. Initial MO concentration = 25 mg/L; reaction time = 25 min; adsorbents dosage = 0.1 g; pH = 7.

In view of the above-mentioned experimental results, kinetic fitting was performed for BFSAP to understand the adsorption process.

Several groups have investigated the adsorption kinetics mechanism of pollutant treatments and reported various kinetic models. Based on the Lagergren first-order kinematic model, the pseudo first-order kinetic equation is expressed as follows:

$$\ln(q_e - q_t) = \ln(q_e) - k_1 t \quad (3)$$

where, k_1 (min^{-1}) is the rate constant of the pseudo first-order model, q_e (mg/g) and q_t (mg/g) are adsorption capacity at equilibrium and at time t respectively. A plot of $\ln(q_e - q_t)$ versus t gives the k_1 and q_e values.

Kinetic data were further analyzed with the pseudo second-order kinetic model in the following linear form:

$$\frac{t}{q_t} = \frac{1}{k_2 q_e^2} + \frac{1}{q_e}(t) \quad (4)$$

where, k_2 (g/(min mg)) is the rate constant of the pseudo second-order model and q_t (mg/g) and q_e (mg/g) are the amount of adsorbate adsorbed at time t and at equilibrium, respectively. The values of constants (k_2 and q_e) can be obtained from the intercept and slope of a linear plot of t/q_t versus t (Dal Bosco, 2005).

From Fig. 10, it can be seen that the adsorption process of BFSAP can be well described with the pseudo-second-order model over a range of initial MO concentrations. This result revealed that the adsorption process might be described as chemisorption rather than diffusion exchange, which is always the rate-limiting step for adsorption.

2.2.5. *Adsorption isotherms*

Based on the Langmuir and Freundlich adsorption equilibrium isotherms, the adsorption process can be divided into single and multi-tiered adsorption. The Langmuir model assumes that both the solution system and adsorbed layer are in a perfect state, and adsorption occurs as a monomolecular layer. The Freundlich

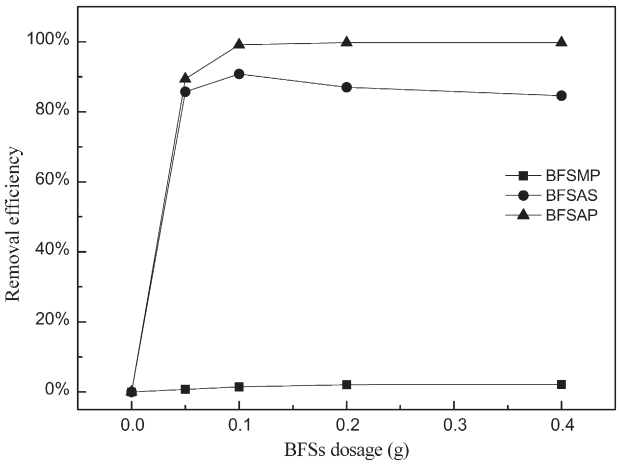

Fig. 5 – Effect of BFS dosage on MO removal efficiency. Initial MO concentration = 25 mg/L; reaction time = 25 min; temperature = 25°C; pH = 7.

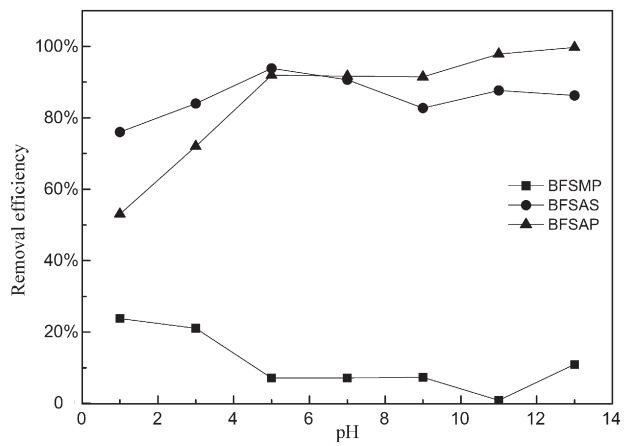

Fig. 7 – Effect of pH on MO adsorption. (Initial MO concentration = 25 mg/L; reaction time = 25 min; temperature = 25°C; adsorbents dosage = 0.1 g).

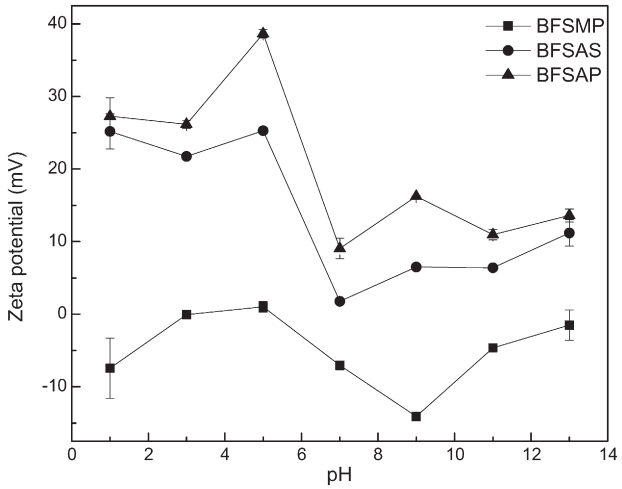

Fig. 8 – The curve graph of zeta potential of BFSMP, BFSAP, and BFSAS.

model assumes that the solid surface is non-uniform, and adsorption occurs in polymolecular layers.

The equation for the Langmuir isotherm is shown below:

$$q_e = \frac{QbC_e}{1 + bC_e} \quad (5)$$

where the coefficient Q (mg/g) denotes the maximum adsorption capacity and b (L/mg) is the Langmuir constant. q_e (mg/g) is mg of adsorbate adsorbed per gram of adsorbent media and C_e (mg/L) is the equilibrium adsorbate concentration in solution. The constants in the Langmuir isotherm can be calculated by plotting $1/q_e$ versus $1/C_e$.

The Freundlich equation is given as:

$$q_e = K_F C_e^{1/n} \quad (6)$$

where, K_F is, roughly, an indicator of the adsorption capacity and $1/n$ is the adsorption intensity. The linear form of the Freundlich expression will yield the constants K_F and $1/n$.

As shown in Figs. 11 and 12, the correlation coefficients of the Langmuir and Freundlich isotherms were 0.999 and 0.893 respectively, indicating that single-layer adsorption occurred in MO removal with BFS. Awual et al. reported that sorption takes place at specific homogeneous sites within materials and the Langmuir model has found successful application in many sorption processes characterized by monolayer sorption (Awual, 2015, 2016; Awual and Hasan, 2015a, 2015b; El-Safty et al., 2011; Awual et al., 2015, 2016). However, the adsorption isotherms for the retention of MO by ZnAl-LDHs or MgAl-LDHs could be described well with the Freundlich equation (Morimoto et al., 2011). This discrepancy may be due to the fact that BFSAP is a mixture of various hydrotalcite phases, and exhibited different adsorptive behavior in MO removal than that of a single hydrotalcite. It can be seen from Table 3 that the maximum MO adsorption on BFSAP was 167 mg/g, which is comparable to that of Ni–Al LDH and Zn–Al LDO, and it performed better than FeOOH/CBC nanocomposite.

2.3. Adsorption mechanism analysis

2.3.1. MO-BFSAP interaction

FT-IR analysis was conducted to understand the underlying mechanism of MO removal by BSFAP adsorption. From Appendix A Fig. S1, it can be observed that the broad band at 648 cm^{-1} in the BFSAP spectrum is caused by various lattice vibrations associated with metal hydroxide sheets. The broad band at 3471 cm^{-1} mainly results from O–H groups on hydroxide layers (Costa et al., 2008). For MO, the C–H aromatic out-of-plane bend occurs at 817 cm^{-1}. The stretching band of 1,4 substituents on the benzene ring occurs at 1157 cm^{-1}. What is more, the C-N bending vibration of the N atom connected with the benzene ring is observed at 1342 cm^{-1}, and the N═N stretching band emerges at 1604 cm^{-1}. The characteristic peak of $-CH_3$ is weakened and shifted at 2869 cm^{-1}. Compared with BFSAP or MO alone, some obvious variations in characteristic absorption peaks were detected. First, the characteristic peak at 786 cm^{-1} originating from C–H aromatic out-of-plane bending shifted, and a peak at 1049 cm^{-1} caused by S═O and SO_3^- groups was also observed.

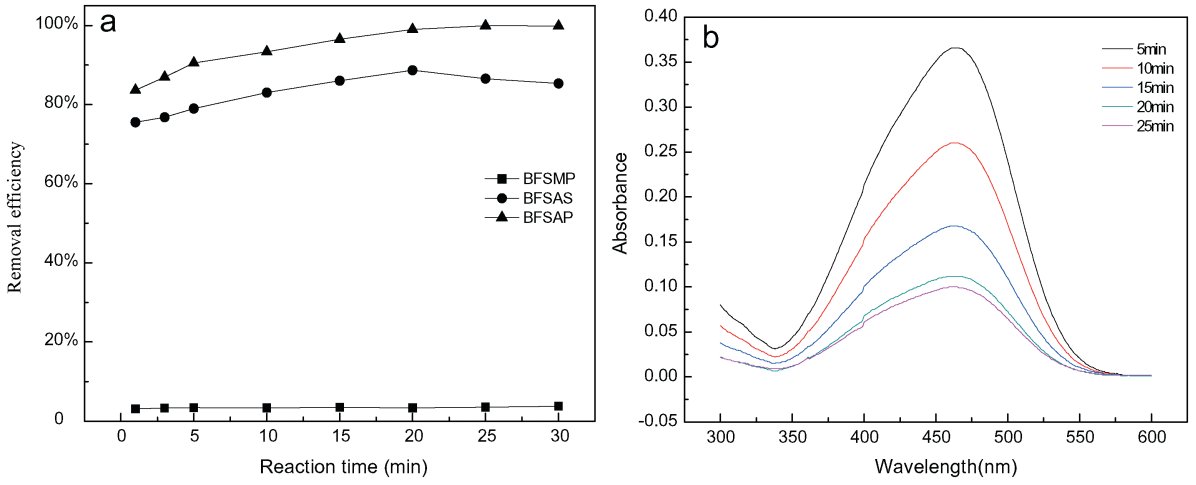

Fig. 9 – The adsorption of BFSMP, BFSAS and BFSAP vs. reaction time (a) and spectral absorption of BFSAP at different reaction times (Initial MO concentration = 25 mg/L; pH = 11; temperature = 25°C; adsorbents dosage = 0.1 g).

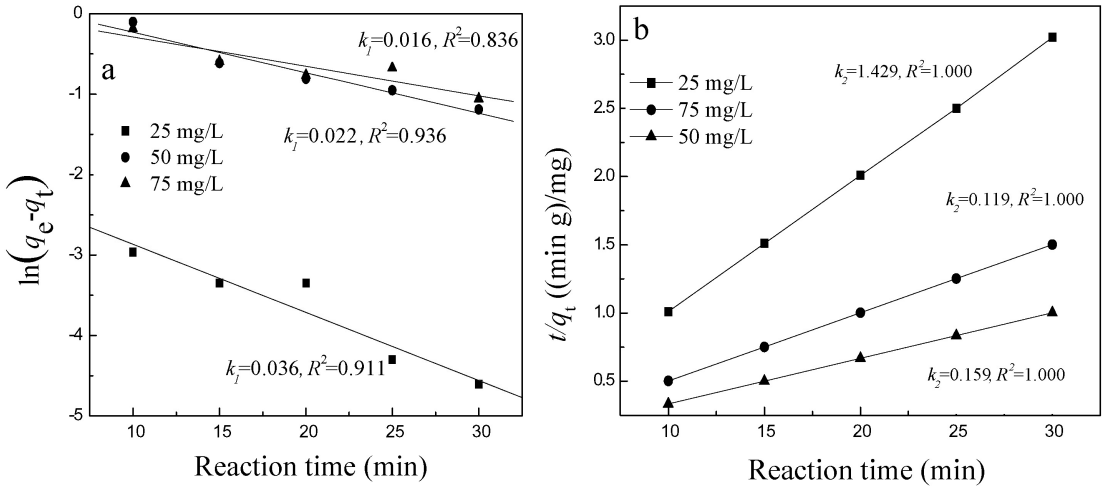

Fig. 10 – The pseudo first-order (a)and pseudo second-order model for the adsorption process of BFSAP.

In addition, the vibration absorption peak of the azo double bond appears at 1403.9 cm^{-1}, and the characteristic peak of $–CH_3$ from C–H antisymmetric stretch occurred at 2946.7 cm^{-1} (Shan et al., 2015; Costa et al., 2009). The peak at 3440 cm^{-1} is due to water bending modes. Similar to the adsorption mechanism of layered double hydroxides (LDHs) for MO removal, replacement of OH– anion in the interlayer region by MO was responsible for its removal (Zhang et al., 2014a, 2014b; Li et al., 2014; Shan et al., 2015). That is to say, MO was removed in BFSAP adsorption through formation BFSAP-MO complexes (Appendix A Fig. S2). The kinetic modeling result was confirmed by FT-IR analysis, showing that chemical adsorption was predominant in MO removal.

In addition, it is interesting to note that the color change intervals for MO solution are orange at pH of 3.1 to 4.4, red at pH less than 3.1 and yellow at pH more than 4.4. The mode of occurrence of MO in neutral and alkaline solution is the sulfonic acid sodium salt, which converts to sulfonic acid in acidic solution. Then the sulfonic group and the intramolecular alkaline acid dimethyl amine form the dimethyl amino phenyl azo benzene sulfonic acid (para quinoid structure). The color changes after a conjugated system containing a para quinone structure is formed. An increasing concentration of OH^- is conducive to facilitating the release of metal ions from BFSAP. It also promoted the adsorption rate of BFSAP for MO removal. Meanwhile, the adsorption rate slightly decreased with increasing temperature. This means that the adsorption of BFSAP on MO is an exothermic reaction. The increased temperature enhanced molecular motion and weakened the adsorptive removal of MO by BFSAP.

Based on the results of the optimized experiments, the results conformed with the Langmuir adsorption isotherm and pseudo-second-order kinetics. This showed that MO removal by BFSAP mainly occurred by chemisorption, and partly by physical adsorption. The size of the MO ion is 6–8 nm. Though BFSAS (245 m^2/g) apparently has much larger specific surface area than BFSAP (3.46 m^2/g), the pore size of BFSAS is smaller than that of BFSAP. However, the number of positive charges on BFSAP was greater than on BFSAS, which was helpful to the absorption of MO^- on BFSAP. Thus the MO removal of BFSAS was slightly worse than BFSAP. In the process of MO removal by BFSAS, a sol phenomenon occurred under low pH conditions.

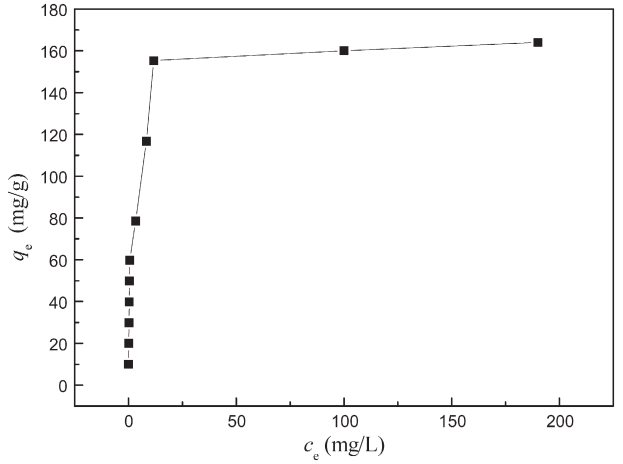

Fig. 11 – The amount of adsorbate adsorbed (q_e) at equilibrium as a function of equilibrium concentrations (C_e).

2.3.2. Effects of inorganic anions on MO removal in BFSAP adsorption

In general, dye wastewater always contains a large amount of inorganic anions, such as chloride ions, sulfate and phosphate, so the effects of inorganic anions on adsorptive removal of MO were investigated. Adsorption experiments were based on the optimum BFSAP dosage of 2 g/L. As depicted in Appendix A Fig. S3, NaCl and $NaNO_3$ had no significant effect on the removal efficiency of MO in BFSAP treatment, but MO removal was reduced in the presence of Na_2SO_4 and Na_3PO_4, and was more evident for Na_3PO_4. This result revealed that SO_4^{2-} and PO_4^{3-} could compete for the adsorption sites located on the surface of BFSAP by an ion-exchange process (Costa et al., 2009).

The influence of the concentration of Na_2SO_4 and Na_3PO_4 on MO removal in BFSAP adsorption is presented in Appendix A Fig. S4. It is clear that MO removal was significantly reduced with increasing concentrations of SO_4^{2-} and PO_4^{3-}. Adsorptive removal of MO sharply decreased from 30.73% to 5.16% on

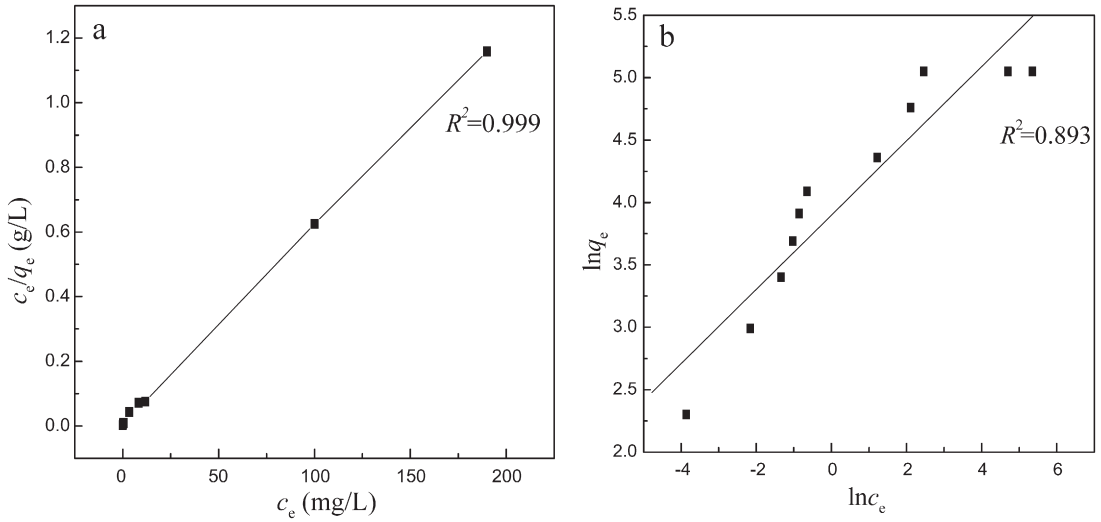

Fig. 12 – Langmuir (a) and Freundlich (b) adsorption isotherm.

increasing the concentration of Na_2SO_4 from 0.005 to 0.05 mol/L. Furthermore, PO_4^{3-} had a more marked influence on the adsorption capacity of BFSAP for MO removal, which was significantly reduced from 27.07% to 0.89% with increase in concentration of Na_3PO_4 from 0.005 to 0.05 mol/L. As mentioned above, it has been reported that both SO_4^{2-} and PO_4^{3-} could be removed by hydrotalcite adsorption (Costa et al., 2009).

The surface functional groups of BFSAP were analyzed with FT-IR after adsorption to understand the mechanism of the inhibitory effects of SO_4^{2-} and PO_4^{3-} on MO removal. The results can be found in Appendix A Fig. S5. In comparison to BFSAP-MO in the absence of inorganic anions, the characteristic peak related to $-CH_3$ weakened and nearly disappeared at 2869 cm^{-1} when the SO_4^{2-} concentration was around 4.8 mg/L. Meanwhile, a broad band at 648 cm^{-1} and characteristic peak at 1049 cm^{-1} associated with SO_4^{2-} were detected. For the BFSAP-MO-PO_4 system, a characteristic peak at 1049 cm^{-1} originating from the P–O group was observed (Yin et al., 2012). These observations demonstrated that the MO removal reduction was attributable to chemisorption (ion-exchange) of SO_4^{2-} and PO_4^{3-}.

From Appendix A Fig. S6, it can be seen that the characteristic peaks of BFSAP-MO, BFSAP-MO-SO_4 and BFSAP-MO-PO_4 all obviously broadened to a variable extent and shifted, which suggested that the interlayer spacing increased. The intensity of the XRD peaks weakened because some metal ions of BFSAP were released into the simulated wastewater during anion exchange reactions, which led to structural change (Kooli et al., 1997; Hibino and Tsunashima, 1997; Serwicka et al., 1997; Radha et al., 2005). Meanwhile, MO, PO_4^{3-} and SO_4^{2-} had a very limited influence on the interlayer structure of BFSAP, which led BFSAP-MO, BFSAP-MO-PO_4 and BFSAP-MO-SO_4 to have weakened crystallinity.

3. Conclusions

As a kind of industrial solid waste, the handling of BFS costs a large sum of money in the iron and steel industry. How to dispose of BFS and gain a high value-added product was the focus of this work.(1) In the study, we adopted a simple technological process, which is a low-cost acid-alkali method. The materials BFSAS and BFSAP were obtained. BFSAS has a large surface area (245 m^2/g) and shows some adsorptive properties. BFSAP is a complex layered double hydroxide mixture and composed of Ca, Mg, Al. (2) BFSAP has been demonstrated to be an effective adsorbent for the removal of MO from aqueous solution. The adsorption process followed the Langmuir isotherm. The adsorption efficiency was very stable with respect to varying contact time, pH and adsorbent dosage. The maximum adsorption capacity of BFSAP for MO reached 167 mg/g.(3) Adsorption of MO from NaCl solution and saturated $NaNO_3$ solution showed little change compared to solution without added anions, while adsorption from Na_2SO_4 solution and saturated Na_3PO_4 solution was markedly reduced.

Acknowledgments

This work was supported by the National Nature Science Foundation of China (Nos. 21277130, 51478445, 51338010 and 21477118) and the Key Program Nature Science Foundation of Hubei Province (No. 2014CFA530), Chinese Universities Scientific Fund (CUG) and China Postdoctoral Science Foundation under 2016M590733.

REFERENCES

Awual, M.R., 2014. Investigation of potential conjugate adsorbent for efficient ultra-trace gold(III) detection and recovery. J. Ind. Eng. Chem. 20 (5), 3493–3501.

Awual, M.R., 2015. A novel facial composite adsorbent for enhanced copper(II) detection and removal from wastewater. Chem. Eng. J. 266, 368–375.

Awual, M.R., 2016. Assessing of lead(III) capturing from contaminated wastewater using ligand doped conjugate adsorbent. Chem. Eng. J. 289, 65–73.

Awual, M.R., Hasan, M.M., 2014a. A novel fine-tuning mesoporous adsorbent for simultaneous lead(II) detection and removal from wastewater. Sensor. Actuat. B: Chem. 202, 395–403.

Awual, M.R., Hasan, M.M., 2014b. Novel conjugate adsorbent for visual detection and removal of toxic lead(II) ions from water. Microp. Mesopor. Mat. 196, 261–269.
Awual, M.R., Hasan, M.M., 2015b. Fine-tuning mesoporous adsorbent for simultaneous ultra-trace palladium(II) detection, separation and recovery. J. Ind. Eng. Chem. 21, 507–515.
Awual, M.R., Hasan, M.M., Khaleque, M.A., 2015. Efficient selenium(IV) detection and removal from water by tailor-made novel conjugate adsorbent. Sensor. Actuat. B: Chem. 209, 194–202.
Awual, M.R., Hasan, M.M., Khaleque, M.A., Sheikh, M.C., 2016. Treatment of copper(II) containing wastewater by a newly developed ligand based facial conjugate materials. Chem. Eng. J. 288, 368–376.
Barbosa, L. V., Marçal, L., Nassar, E. J., Calefi, P. S., Vicente, M. A., Trujillano, R.et al., 2015. Kaolinite-titanium oxide nanocomposites prepared *via* sol–gel as heterogeneous photocatalysts for dyes degradation. Cata. Today, 2015. 246: p. 133–142.
Chen, Q., Liu, H., 2007. Comprehensive utilization of solid wastes discharged from iron and steel industry. Min. Metall. Eng. 3, 012.
Costa, F.R., Leuteritz, A., Wagenknecht, U., Jehnichen, D., Haeussler, L., Heinrich, G., 2008. Intercalation of Mg–Al layered double hydroxide by anionic surfactants: preparation and characterization. Appl. Clay Sci. 38 (3–4), 153–164.
Costa, F.R., Leuteritz, A., Wagenknecht, U., der Landwehr, M.A., Jehnichen, D., Haeussler, L., et al., 2009. Alkyl sulfonate modified LDH: effect of alkyl chain length on intercalation behavior, particle morphology and thermal stability. Appl. Clay Sci. 44 (1–2), 7–14.
Dal Bosco, S.M., JimenezR.S., Carvalho W.A., 2005. Removal of toxic metals from wastewater by Brazilian natural scolecite. J. Colloid Int. Sci. 281(2), 424–431.
Dou, P., Tan, F., Wang, W., Sarreshteh, A., Qiao, X., Qiu, X., 2015. One-step microwave-assisted synthesis of Ag/ZnO/graphene nanocomposites with enhanced photocatalytic activity. J. Photoch. Photobio. A. 302, 17–22.
El-Safty, S.A., Shahat, A., Awual, M.R., 2011. Efficient adsorbents of nanoporous aluminosilicate monoliths for organic dyes from aqueous solution. J. Colloid Int. Sci. 359 (1), 9–18.
Fan, Y., Liu, H.J., Zhang, Y., Chen, Y., 2015. Adsorption of anionic MO or cationic MB from MO/MB mixture using polyacrylonitrile fiber hydrothermally treated with hyperbranched polyethylenimine. J. Hazard. Mater. 283, 321–328.
Awual, M. R, Hasan, M. M., 2015a. Colorimetric detection and removal of copper(II) ions from wastewater samples using tailor-made composite adsorbent. Sensor. Actuat. B: Chem. 206, 692–700.
Hibino, T., Tsunashima, A., 1997. Synthesis of paramolybdate intercalates of hydrotalcite-like compounds by ion exchange in ethanol/water solution. Chem. Mater. 9 (10), 2082–2089.
Kooli, F., Jones, W., Rives, V., Ulibarri, M.A., 1997. An alternative route to polyoxometalate-exchanged layered double hydroxides: the use of ultrasound. J. Mater. Sci. Letters. 16 (1), 27–29.
Kuwahara, Y., Yamashita, H., 2015. Synthesis of Ca-based layered double hydroxide from blast furnace slag and its catalytic applications. ISIJ Int. 55 (7), 1531–1537.
Kuwahara, Y., Ohmichi, T., Kamegawa, T., Mori, K., Yamashita, H., 2010. A novel conversion process for waste slag: synthesis of a hydrotalcite-like compound and zeolite from blast furnace slag and evaluation of adsorption capacities. J. Mater. Chem. 20 (24), 5052–5062.
Kuwahara, Y., Tamagawa, S., Fujitani, T., Yamashita, H., 2013. A novel conversion process for waste slag: synthesis of calcium silicate hydrate from blast furnace slag and its application as a versatile adsorbent for water purification. J. Mate. Chem. A.1, 7199–7210.
Li, Z., Yang, B., Zhang, S., Wang, B., Xue, B., 2014. A novel approach to hierarchical sphere-like ZnAl-layered double hydroxides and their enhanced adsorption capability. J. Mater. Chem. A 2 (26), 10202–10210.
Monash, P., Pugazhenthi, G., 2014. Utilization of calcined Ni–Al layered double hydroxide (LDH) as an adsorbent for removal of methyl orange dye from aqueous solution. Env. Progr. Sust. Energ. 33 (1), 154–159.
Morimoto, K., Tamura, K., Iyi, N., Ye, J., Yamada, H., 2011. Adsorption and photodegradation properties of anionic dyes by layered double hydroxides. J. Phys. Chem. Solids 72 (9), 1037–1045.
Ni, Z.M., Xia, S.J., Wang, L.G., Xing, F.F., Pan, G.X., 2007. Treatment of methyl orange by calcined layered double hydroxides in aqueous solution: adsorption property and kinetic studies. J. Colloid Int. Sci. 316 (2), 284–291.
Radha, A.V., Kamath, P.V., Shivakumara, C., 2005. Mechanism of the anion exchange reactions of the layered double hydroxides (LDHs) of Ca and Mg with Al. Solid State Sci. 7 (10), 1180–1187.
Ren, Q. Q., Hao, S. J., Jiang, W. F., Zhang, Y. Z., Zhang, W. P., 2014. Study of comprehensive utilization on Ti-bearing blast furnace Slag, in Appl. Mech. Mat., H.W. Liu, H.W. Liu^Editors. pp. 141–144.
Serwicka, E.M., Nowak, P., Bahranowski, K., Jones, W., Kooli, F., 1997. Insertion of electrochemically reduced Keggin anions into layered double hydroxides. J. Mater. Chem. 7 (9), 1937–1939.
Shan, R.R., Yan, L.G., Yang, Y.M., Yang, K., Yu, S.J., Yu, H.Q., et al., 2015. Highly efficient removal of three red dyes by adsorption onto Mg–Al-layered double hydroxide. J. Ind. Eng. Chem. 21, 561–568.
Wang, J.J., Jing, Y.H., Ouyang, T., Chang, C.T., 2015a. Preparation of 13× from waste quartz and photocatalytic reaction of methyl orange on TiO_2/ZSM-5,13X and Y-zeolite. J. Nanosci. Nanotechno. 15 (8), 6141–6149.
Wang, Z., Ma, Y., He, H., Pei, C., He, P., 2015b. A novel reusable nanocomposite: FeOOH/CBC and its adsorptive property for methyl orange. Appl. Surf. Sci. 332, 456–462.
Yan, Z.W., 2012. Discussion on progress of energy saving and emission reduction in TISCO. Iron & Steel. 12, 016.
Yang, X.L., Dai, H.X., Li, X., 2013. Comprehensive utilization and discussion of iron and steel metallurgical slag. Adv. Mat. Res. 807, 2328–2331.
Yin, L., Lei, G.Y., Li, C.J., Liu, Z.J., 2012. Adsorption of phosphate by calcined Mg–Al–Fe layered double hydroxides. Environ. Chem. 31 (7), 1050–1055.
Zhang, P., Wang, T., Qian, G., Wu, D., Frost, R.L., 2014a. Removal of methyl orange from aqueous solutions through adsorption by calcium aluminate hydrates. J. Colloid Int. Sci. 426, 44–47.
Zhang, C., Yang, S., Chen, H., He, H., Sun, C., 2014b. Adsorption behavior and mechanism of reactive brilliant red X-3B in aqueous solution over three kinds of hydrotalcite-like LDHs. Appl. Surf. Sci. 301(SI), 329–337.
Zheng, H., Qin, L., Lin, H., Nie, M., Li, Y., Li, Q., 2015. Convenient route to well-dispersed Cu_2O Nanospheres and their use as photocatalysts. J. Nanosci. Nanotechno. 15 (8), 6063–6068.